Journal of Biomedical Optics

BiomedicalOptics.SPIEDigitalLibrary.org

Evaluation of light scattering and absorption properties of *in vivo* rat liver using a single-reflectance fiber probe during preischemia, ischemia–reperfusion, and postmortem

Sharmin Akter
Satoshi Maejima
Satoko Kawauchi
Shunichi Sato
Akinari Hinoki
Suefumi Aosasa
Junji Yamamoto
Izumi Nishidate

SPIE.

Evaluation of light scattering and absorption properties of *in vivo* rat liver using a single-reflectance fiber probe during preischemia, ischemia–reperfusion, and postmortem

Sharmin Akter,[a] Satoshi Maejima,[b] Satoko Kawauchi,[c] Shunichi Sato,[c] Akinari Hinoki,[b] Suefumi Aosasa,[b] Junji Yamamoto,[b] and Izumi Nishidate[a,*]

[a]Tokyo University of Agriculture and Technology, Graduate School of Bio-Application and Systems Engineering, 2-24-16, Naka-cho, Koganei, Tokyo 184-8588, Japan
[b]National Defense Medical College, Department of Surgery, 3-2, Namiki, Tokorozawa, Saitama 359-8513, Japan
[c]National Defense Medical College Research Institute, Division of Biomedical Information Sciences, 3-2, Namiki, Tokorozawa, Saitama 359-8513, Japan

Abstract. Diffuse reflectance spectroscopy (DRS) has been extensively used for characterization of biological tissues as a noninvasive optical technique to evaluate the optical properties of tissue. We investigated a method for evaluating the reduced scattering coefficient μ_s', the absorption coefficient μ_a, the tissue oxygen saturation StO_2, and the reduction of heme *aa*3 in cytochrome c oxidase CcO of *in vivo* liver tissue using a single-reflectance fiber probe with two source-collector geometries. We performed *in vivo* recordings of diffuse reflectance spectra for exposed rat liver during the ischemia–reperfusion induced by the hepatic portal (hepatic artery, portal vein, and bile duct) occlusion. The time courses of μ_a at 500, 530, 570, and 584 nm indicated the hemodynamic change in liver tissue as well as StO_2. Significant increase in $\mu_a(605)/\mu_a(620)$ during ischemia and after euthanasia induced by nitrogen breathing was observed, which indicates the reduction of heme *aa*3, representing a sign of mitochondrial energy failure. The time courses of μ_s' at 500, 530, 570, and 584 nm were well correlated with those of μ_a, which also reflect the scattering by red blood cells. On the other hand, at 700 and 800 nm, a temporary increase in μ_s' and an irreversible decrease in μ_s' were observed during ischemia–reperfusion and after euthanasia induced by nitrogen breathing, respectively. The change in μ_s' in the near-infrared wavelength region during ischemia is indicative of the morphological changes in the cellular and subcellular structures induced by the ischemia, whereas that after euthanasia implies the hepatocyte vacuolation. The results of the present study indicate the potential application of the current DRS system for evaluating the pathophysiological conditions of *in vivo* liver tissue. [DOI: 10.1117/1.JBO.20.7.076010]

Keywords: diffuse reflectance spectroscopy; Monte Carlo simulation; absorption coefficient; reduced scattering coefficient; tissue oxygen saturation; liver ischemia–reperfusion.

Paper 150222R received Apr. 3, 2015; accepted for publication Jun. 25, 2015; published online Jul. 27, 2015.

1 Introduction

Liver ischemia–reperfusion involves a complex series of processes that may culminate in hepatocellular injury. Liver ischemia–reperfusion is a common consequence of liver surgery, particularly after hepatectomy and liver transplantation, complicated by microcirculatory liver failure, followed by necrosis and cell death.[1] Occlusion of hepatic inflow (Pringle maneuver) by portal vein clamping was initially devised to reduce intraoperative blood loss during emergency liver resection.[2] The important side effect of partial liver resection is the ischemia in the remnant liver following temporary vascular occlusion.[3] The liver contains many more chromophores [oxygenated hemoglobin (HbO), deoxygenated hemoglobin (HbR), cytochrome c oxidase (CcO), lipid, water, etc.] than other organs. Since liver function depends greatly upon the oxygen supply, it is clinically important to monitor the oxygenation state of the liver in patients after liver surgery. In the present study, we demonstrate the characterization of the light scattering and absorption properties of *in vivo* liver tissue based on diffuse reflectance spectroscopy (DRS). DRS is a promising method of detecting the macroscopic information of tissue samples, such as the scattering property, the total hemoglobin concentration, and the tissue oxygen saturation of hemoglobin (StO_2).[4,5] Near-infrared (NIR) spectroscopy has been reported to be useful in detecting the oxygenation state of the graft liver after transplantation, and the StO_2 value can be an indicator of the patient's prognosis.[6,7] The recent development of DRS has made it possible to determine the absorption coefficient μ_a and the reduced scattering coefficient μ_s' of a tissue independently. The absorption coefficient μ_a is defined as the probability of photon absorption per unit infinitesimal path length, and the reduced scattering coefficient μ_s' is defined as the probability of photon scattering per unit infinitesimal path length.[8] DRS is an optical measurement technique that records changes in the spectral distribution of light after its interaction with the tissue. Changes in the diffuse reflectance spectra are primarily a result of the combination of absorption and scattering of light for each wavelength of light produced by a broadband light source. Light absorption is primarily related to chromophore contents of tissue, whereas light scattering is influenced primarily by cellular and subcellular structures of tissue. The total light absorption is the sum of the absorption due to

*Address all correspondence to: Izumi Nishidate, E-mail: inishi@cc.tuat.ac.jp;

1083-3668/2015/$25.00 © 2015 SPIE

endogenous chromophores.[9] HbO and HbR are the primary absorbers in biological tissues in the visible wavelength region,[10] whereas the dominant absorbers in the NIR wavelength region are lipids, water, and collagen.[11] The severity of liver ischemia–reperfusion injury can be reliably assessed by measuring changes in HbO, HbR, and the redox state of heme *aa*3 in CcO.[9] By illuminating tissue with a selected spectral band of light and subsequent analysis of the characteristic scattering and absorption patterns, it is possible to obtain an "optical fingerprint" of the tissue. Such an optical fingerprint represents specific quantitative biochemical and morphological information from the examined tissue and may depend on the metabolic rate, vascularity, intravascular oxygenation, and alterations in tissue morphology.[12] DRS has been used for tissue surface analysis during endoscopical procedures and analysis of tissue abnormalities in solid organs.[13] Light scattering and absorption properties of *in vivo* tissues can be evaluated by several noninvasive methods, such as time-resolved measurements,[14] a frequency-domain method,[15] optical coherence methods,[16] a pulsed photothermal radiometry method,[17] and spatially resolved measurements.[18–21] DRS based on the spatially resolved measurements with continuous-wave light can be simply achieved with a white light source, inexpensive optical components, and a spectrometer. The primary notable changes within a light spectrum after interaction with tissue are a result of either the absorption or scattering of light. Using various mathematical models, the spectral characteristics of the absorption coefficient $\mu_a(\lambda)$ and the reduced scattering coefficient $\mu_s'(\lambda)$ can be extracted from the measured reflectance spectrum.[22] DRS using a fiber optic probe is a promising technique for monitoring tissue oxygenation, demonstrating promising results in the discrimination of malignant lesions from normal tissue[23–26] and assessment of tissue viability.[27] In addition, DRS has been demonstrated to identify irreversible cell damage during radiofrequency ablation,[28] severe steatosis, and hepatitis, thereby preventing overly extensive resections in these high-risk patients.[29–32] Furthermore, DRS could potentially be used intraoperatively for the assessment of bowel viability in real time.[33] Various source-collector geometries have been used to estimate the reduced scattering coefficient μ_s' and the absorption coefficients μ_a in DRS with a fiber-optic probe.[18,26,33–36] Moreover, a single-reflectance fiber probe will be easy to use for practical uses, especially in clinical situations. Nevertheless, to our knowledge, information regarding measurement of ischemia–reperfusion injury using a DRS system is very limited.

In the present study, we use a simple DRS system previously developed by Nishidate et al.[37] to estimate the reduced scattering coefficient spectrum $\mu_s'(\lambda)$ and the absorption coefficient spectrum $\mu_a(\lambda)$ of *in vivo* biological tissue. In order to confirm the validity of the method for evaluating changes in the optical properties of *in vivo* liver tissue, we performed *in vivo* experiments using exposed rat liver before and during ischemia–reperfusion induced by the occlusion of the hepatic portal as well as postmortem.

2 Principle

2.1 *Reflectance Fiber Probe System*

Figure 1 shows a schematic diagram of the single-reflectance fiber probe system with the two source-collection geometries used in the present study. The system consists of a reflectance fiber probe, bifurcated fiber, a light source, and two spectrometers under the control of a personal computer. The bifurcated

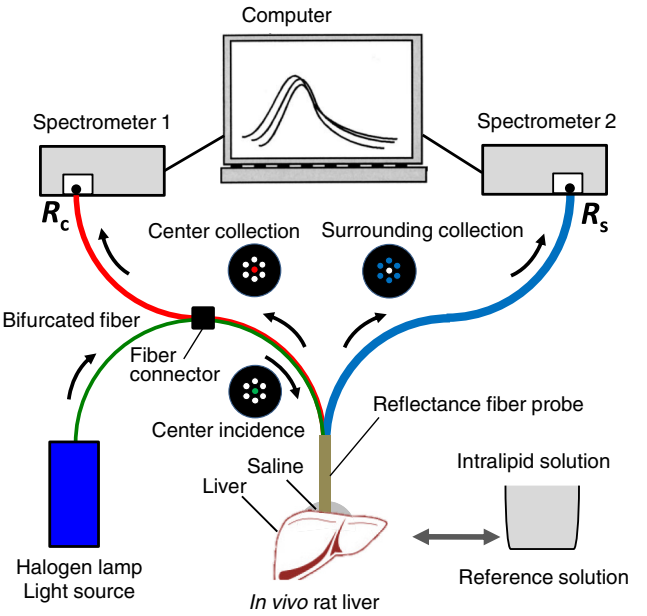

Fig. 1 Single-fiber probe system for measuring the diffuse reflectance spectra with two source-collection geometries setup.

fiber has two optical fibers of the same diameter of 400 μm placed side by side in the common end. The reflectance fiber probe has one 600-μm-diameter fiber in the center surrounded by six 600-μm-diameter fibers. One end of the center fiber of the reflectance probe is connected to the common end of the bifurcated fiber through a fiber connector. A halogen lamp light (HL-2000, Ocean Optics Inc., Dunedin, Florida), which covers the visible to NIR wavelength range, is used to illuminate the sample via one lead of the bifurcated fiber and the central fiber of the reflectance probe. Diffusely reflected light from the sample is collected by both the central fiber and the six surrounding fibers. The center-to-center distances between the surrounding fibers and the central fiber are 700 μm. The light collected by the central fiber is delivered to a multichannel spectrometer (USB4000, Ocean Optics Inc.) via another lead of the bifurcated fiber, whereas the light collected by the six surrounding fibers is delivered to a different multichannel spectrometer (USB4000, Ocean Optics Inc.). A solution of Intralipid 10%[38] was prepared in order to calibrate the spectral responses of both spectrometers as a reference solution. Diffuse reflectance spectra $R_c(\lambda)$ and $R_s(\lambda)$ ranging from 500 to 800 nm were calculated from the spectral intensities of light collected by the central fiber and the six surrounding fibers, respectively, based on the reflected intensity spectra from the reference solution.

2.2 *Determination of Empirical Formulas for Estimating μ_s' and μ_a*

In order to estimate μ_s' and μ_a from the measurements of R_c and R_s, we consider the following equation based on the results of the Monte Carlo simulation:

$$\begin{bmatrix} \mu_s' \\ \mu_a \end{bmatrix} = \begin{bmatrix} \alpha_c & \alpha_s \\ \beta_c & \beta_s \end{bmatrix} \begin{bmatrix} A_c \\ A_s \end{bmatrix}, \tag{1}$$

where $A_c = -\log_{10} R_c$ and $A_s = -\log_{10} R_s$ are the apparent absorbances for the recording by the center fiber and the surrounding fibers, respectively. In order to improve the accuracy

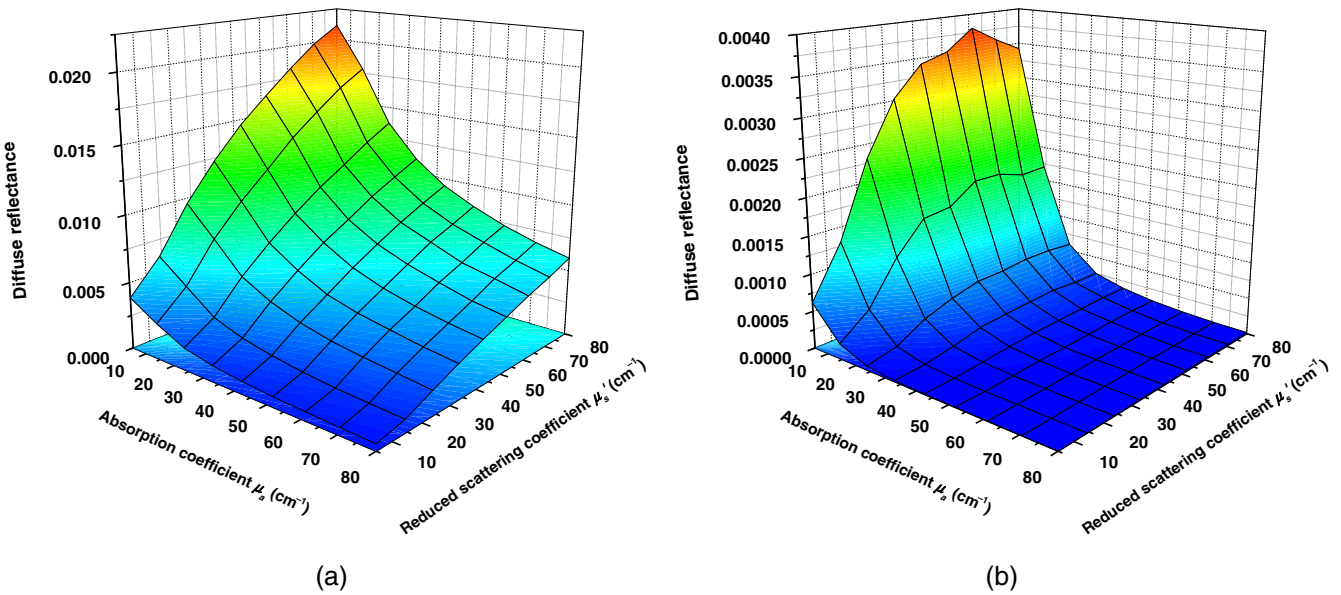

Fig. 2 Results obtained from the Monte Carlo simulations for (a) R_c collected by the center fiber and (b) R_s collected by the surrounding six fibers.

of Eq. (1), we used the higher order terms of A_c and A_s in Eq. (1) as follows:

$$\begin{bmatrix} \mu_s' \\ \mu_a \end{bmatrix} = \begin{bmatrix} \alpha_0 & \alpha_1 & \alpha_2 & \alpha_3 & \alpha_4 & \alpha_5 \\ \beta_0 & \beta_1 & \beta_2 & \beta_3 & \beta_4 & \beta_5 \end{bmatrix} \times \begin{bmatrix} 1 & A_c^2 & A_s^2 & A_c A_s & A_c & A_s \end{bmatrix}^t, \quad (2)$$

where coefficients α_i and β_i $(i = 0, 1, 2, 3, 4, 5)$ in Eq. (2) can be determined statistically by multiple regression analysis of the results of the Monte Carlo simulations, and $[]^t$ represents the transposition of a vector. The details of the Monte Carlo simulation model were published previously.[37] In the Monte Carlo simulations, R_c and R_s were calculated for the ranges of $\mu_a = 0.1$ to 80 cm^{-1} and $\mu_s' = 5.0$. The values of $\mu_s'(\lambda)$ and $\mu_a(\lambda)$ can be estimated by applying Eq. (2) to each wavelength point of $A_c(\lambda)$ and $A_s(\lambda)$. Figures 2(a) and 2(b) show the results obtained from the Monte Carlo simulations for R_c and R_s, respectively. The value of R_c increases monotonically as μ_s' increases, whereas R_s reaches a plateau for larger values of μ_s'. Both R_c and R_s decrease exponentially as μ_a increases, but the effect is more pronounced for R_s. Figure 3 shows the estimated and given values of the reduced scattering coefficient μ_s' [Fig. 3(a)] and the absorption coefficient μ_a obtained from the preliminary numerical investigations [Fig. 3(b)]. In both Figs. 3(a) and 3(b), the estimated values will agree with the given values for the given ranges of μ_s' and μ_a. The coefficient of determination r^2 for μ_a and μ_s' was 0.996 and 0.994, respectively, which indicates a good regression.

2.3 *Evaluation of Tissue Oxygen Saturation and Redox State of Heme aa3 in Cytochrome c Oxidase from* $\mu_a(\lambda)$

The absorption coefficient spectrum is given by the sum of absorption due to oxygenated and deoxygenated hemoglobin. Using the absorption coefficient spectrum $\mu_a(\lambda)$ as a response variable and the extinction coefficient spectra of $\varepsilon_{HbO}(\lambda)$ and

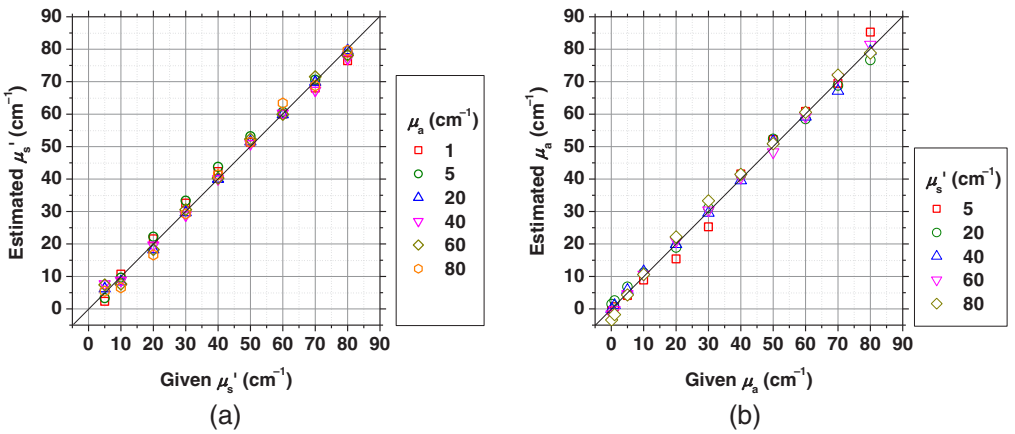

Fig. 3 Estimated and given values obtained from the numerical investigations for (a) the reduced scattering coefficient μ_s' and (b) the absorption coefficient μ_a.

$\varepsilon_{\mathrm{Hb}}(\lambda)$[39] as predictor variables, the multiple regression model can be expressed as:

$$\mu_{\mathrm{a}}(\lambda_k) = a_{\mathrm{HbO}} \times \varepsilon_{\mathrm{HbO}}(\lambda_k) + a_{\mathrm{Hb}} \times \varepsilon_{\mathrm{Hb}}(\lambda_k) + a_0 + e(\lambda_k), \tag{3}$$

where a_{HbO}, a_{Hb}, and a_0 are the regression coefficients, $e(\lambda_k)$ is an error component, and λ_k indicates discrete values in the wavelength range treated in the analysis. By executing the multiple regression analysis for one sample of the absorption coefficient spectrum consisting of p discrete wavelengths, one set of the three regression coefficients is obtained. In this case, the regression coefficient a_0 is a constant component or an intercept and is expressed as:

$$a_0 = \bar{\mu}_a - \bar{\varepsilon}_{\mathrm{HbO}} \cdot a_{\mathrm{HbO}} - \bar{\varepsilon}_{\mathrm{HbR}} \cdot a_{\mathrm{HbR}},$$

where $\bar{\mu}_{\mathrm{a}}$, $\bar{\varepsilon}_{\mathrm{HbO}}$, and $\bar{\varepsilon}_{\mathrm{HbR}}$ are the averages of $\mu_{\mathrm{a}}(\lambda_k)$, $\varepsilon_{\mathrm{HbO}}(\lambda_k)$, and $\varepsilon_{\mathrm{HbR}}(\lambda_k)$ over the wavelength range, or $k = 1$ to p. In the present study, we used the spectral data in the range from 500 to 600 nm at intervals of 10 nm for the multiple regression analysis because the spectral features of oxygenated and deoxygenated hemoglobin notably appear in this wavelength range. The regression coefficients a_{HbO} and a_{Hb} describe the degree of contributions of $\varepsilon_{\mathrm{HbO}}(\lambda)$ and $\varepsilon_{\mathrm{Hb}}(\lambda)$, respectively, to the absorption coefficient spectrum $\mu_{\mathrm{a}}(\lambda)$ and, consequently, are closely related to the concentrations of C_{HbO} and C_{Hb}, respectively. The oxygen saturation of hemoglobin, StO_2, is defined as the percentage of concentration of oxygenated hemoglobin in the concentration of total hemoglobin. In this study, the oxygen saturation is estimated from the regression coefficients a_{HbO} and a_{Hb} as follows:

$$\mathrm{StO}_2[\%] = \frac{a_{\mathrm{HbO}}}{a_{\mathrm{HbO}} + a_{\mathrm{Hb}}} \times 100. \tag{5}$$

We also used the estimated absorption coefficient spectrum $\mu_{\mathrm{a}}(\lambda)$ to evaluate the redox state of heme *aa*3 in CcO. There is an isosbestic point of heme *aa*3 around 620 nm, where the absorption of light by the reduced heme *aa*3 and oxidized heme *aa*3 take the same value, while the absorption spectrum of the reduced heme *aa*3 is maximized at 605 nm.[40] The ratio of absorption at 605 nm and that at 620 nm can be used to evaluate the redox state of heme *aa*3, which indicates the state of mitochondrial energy metabolism. Therefore, in the present study, we evaluate the redox state of heme *aa*3 based on the ratio of the estimated absorption coefficient at 605 nm and that at 620 nm as $\mu_{\mathrm{a}}(605)/\mu_{\mathrm{a}}(620)$.

In order to justify the use of $\mu_{\mathrm{a}}(605)/\mu_{\mathrm{a}}(620)$ to represent the redox state of heme *aa*3 in CcO of liver tissue, we performed the preliminary experiments with an *in vitro* excised liver sample. A normal saline was infused into the excised liver via the portal vein to remove blood from the liver tissue. The oxidation of heme *aa*3 in CcO was induced by continuous infusion of a saline saturated with 95% O_2–5% CO_2 into the liver via the portal vein and subsequent submersion of the liver sample into the saline saturated with 95% O_2–5% CO_2. The reduction of heme *aa*3 in CcO was induced by submersing the liver sample into the mixture of normal saline and a sodium dithionite ($Na_2S_2O_4$). Figure 4 shows the estimated absorption coefficient spectra $\mu_{\mathrm{a}}(\lambda)$ normalized at 620 nm obtained from the excised liver sample submerged into the saline saturated with 95% O_2–5% CO_2 and the mixture of saline and $Na_2S_2O_4$. The normalized absorption at 605 nm under the hyperoxic condition is higher than that treated with $Na_2S_2O_4$, which corresponds to the absorption change due to the reduction of heme *aa*3 in CcO reported in literature.[40]

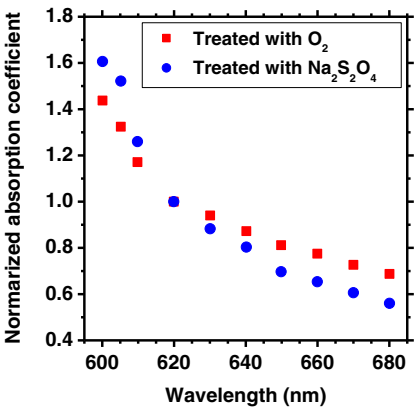

Fig. 4 Estimated absorption coefficient spectra normalized at 620 nm obtained from the excised rat liver sample submerged into the saline saturated with 95% O_2–5% CO_2 (red square) and the mixture of saline and $Na_2S_2O_4$ (blue circle).

3 Experiments

3.1 *Validation of the Method Using Optical Phantoms*

Before the *in vivo* experiments, the experiments with optical phantoms were carried out to validate the empirical model. The phantoms were prepared using Intralipid stock solution (Fresenius Kabi AB, Sweden) as scattering materials. We prepared the scattering solutions by diluting Intralipid stock solution with saline. Hemoglobin solution extracted from red blood cells of horse blood was used as an absorber for lower values of μ_{a}, whereas an India ink (R591217, Rotring, Germany) was used for higher values of μ_{a}. The absorption coefficients of hemoglobin and India ink were experimentally determined based on the transmittance measurements of the hemoglobin solution and India ink solution, respectively, using a cuvette and a spectrometer. The reduced scattering coefficients of Intralipid solutions were evaluated based on the published values.[38] We produced 22 phantoms with ranges of $\mu_{\mathrm{a}} = 0.2$ to 93.6 cm^{-1} and $\mu_{\mathrm{s}}' = 10.3$ to 80.4 cm^{-1} in the wavelength range from 500 to 900 nm to compare the estimated and given optical properties.

3.2 *Animal Experiments*

Six male Wister rats weighing from 150 to 300 g were maintained at 27°C with a 12-/12-h dark/light cycle and allowed food and water *ad libitum*. Experiments performed in the present study were approved by the Animal Research Committee of Tokyo University of Agriculture and Technology. Rats were anesthetized by intraperitoneal injection of a mixture of α-chloralose (50 mg/kg) and urethane (600 mg/kg). A rat model with ischemia–reperfusion to 90% of the liver (Fig. 5) was used.[41] After laparotomy was performed by a transversal injection, the ligaments around the liver lobes were dissected in order to mobilize the left lobe. At the same time, the hepatoduodenal ligament was taped in preparation for further clamping. Before induction of ischemia, the diffuse reflectance spectra of liver

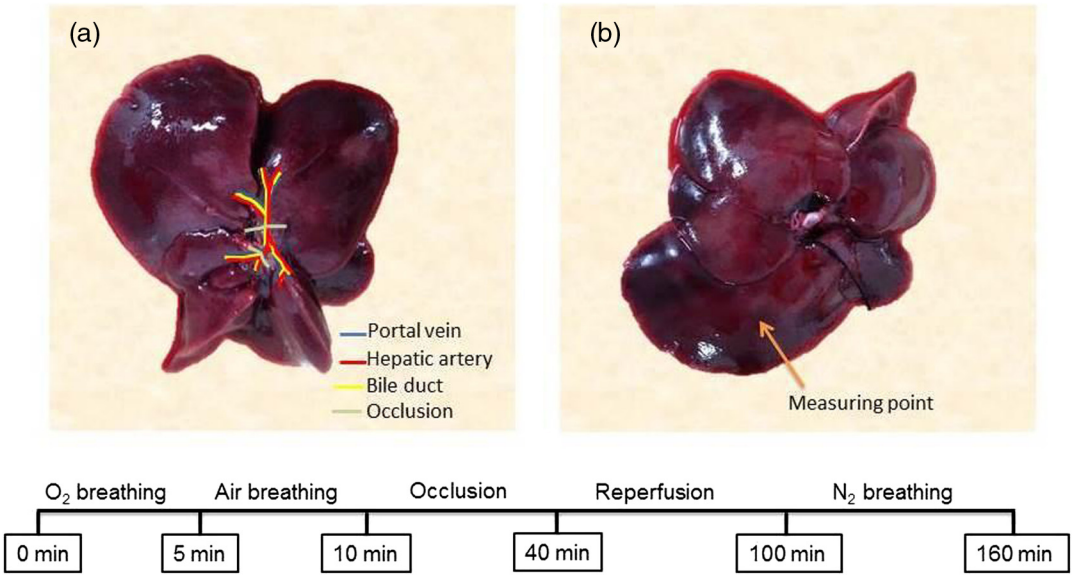

Fig. 5 Graphical illustration of the surgical operation on the rat liver and the protocol in the present study. (a) Schematic drawing representing the ischemic model of the rat liver by blood inflow occlusion on the pedicles of the left lobe, the median lobe, and the right lobe, with no occlusion of the caudate lobe, which is kept as a passage for the portal blood. (b) The dorsal surface of the liver lobe is used for the measurement sites for the diffuse reflectance spectra of the liver.

tissue were recorded as baseline values. Hepatic ischemia was induced by clamping the hepatic portal (the hepatic artery, the portal vein, and the bile duct) for 30 min, followed by declamping. Anoxia was induced by nitrogen breathing at 60 min after the onset of reperfusion ($t = 100$ min). The caudate lobe of the liver was kept as a passage for the portal blood. The reflectance fiber probe was placed on the surface of the liver lobe. Measurements of $R_c(\lambda)$ and $R_s(\lambda)$ were obtained simultaneously in the wavelength range from 500 to 800 nm at 30-s intervals for 160 min: oxygen breathing for 5 min, normal air breathing for 5 min, ischemia for 30 min, reperfusion for 60 min, and nitrogen breathing for 60 min. In order to identify the respiration arrest or euthanasia, the respiration of the rat was confirmed by observing the periodic movement of the lateral region of the abdomen during the experiments. The estimations of $\mu_s'(\lambda)$ and $\mu_a(\lambda)$ were performed based on the process described above. Data are presented as mean $\pm$ SD. An unpaired t-test was performed in order to compare the average values over the samples between the normal (air breathing) and the other periods (oxygen breathing, ischemia, reperfusion, and nitrogen breathing) and $P < 0.05$ was considered significant.

4 Results

4.1 *Validation of the Method Using Optical Phantoms*

Figure 6 shows the estimated and given values for (a) the reduced scattering coefficient μ_s' and (b) the absorption coefficient μ_a, obtained from the phantom experiments. Reasonable results were obtained for both μ_s' and μ_a. Correlation coefficients between the estimated and given values are

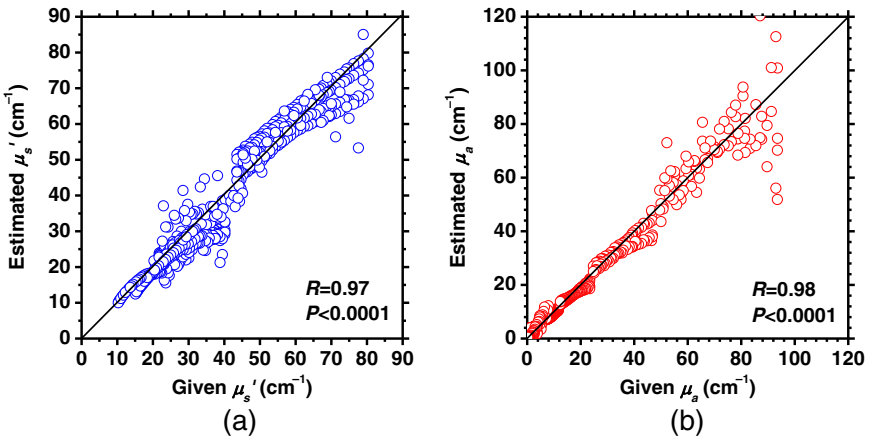

Fig. 6 Estimated and given values obtained from the phantom experiments for (a) the reduced scattering coefficient μ_s' and (b) the absorption coefficient μ_a.

$R = 0.97$ ($P < 0.0001$) and $R = 0.98$ ($P < 0.0001$) for μ_s' and μ_a, respectively. The average root mean square error for μ_s' is $9.2 \pm 8.0\%$ and that for μ_a is $34.9 \pm 45.6\%$. The empirical model yields, in principle, good results for both μ_s' and μ_a, as shown in Figs. 3(a) and 3(b). In Fig. 6(b), however, the estimated error for μ_a increases as the given value increases, which could be attributed to the fact that the current simulation model does not accurately represent the actual experimental conditions, e.g., the distance between the central and surrounding fibers is not accurately taken into consideration.

4.2 *Animal Experiments*

Figure 7 shows the time courses of μ_a averaged over the six samples at specific wavelengths during the period of preischemia (oxygen breathing and air breathing), ischemia, reperfusion, and nitrogen breathing. The error bars in Fig. 7 represent the standard deviation over the six samples. The average values of μ_a over the six samples at each wavelength are averaged over each period and are summarized in Table 1. The baseline absorption coefficients at 530 and 570 nm are noticeably higher

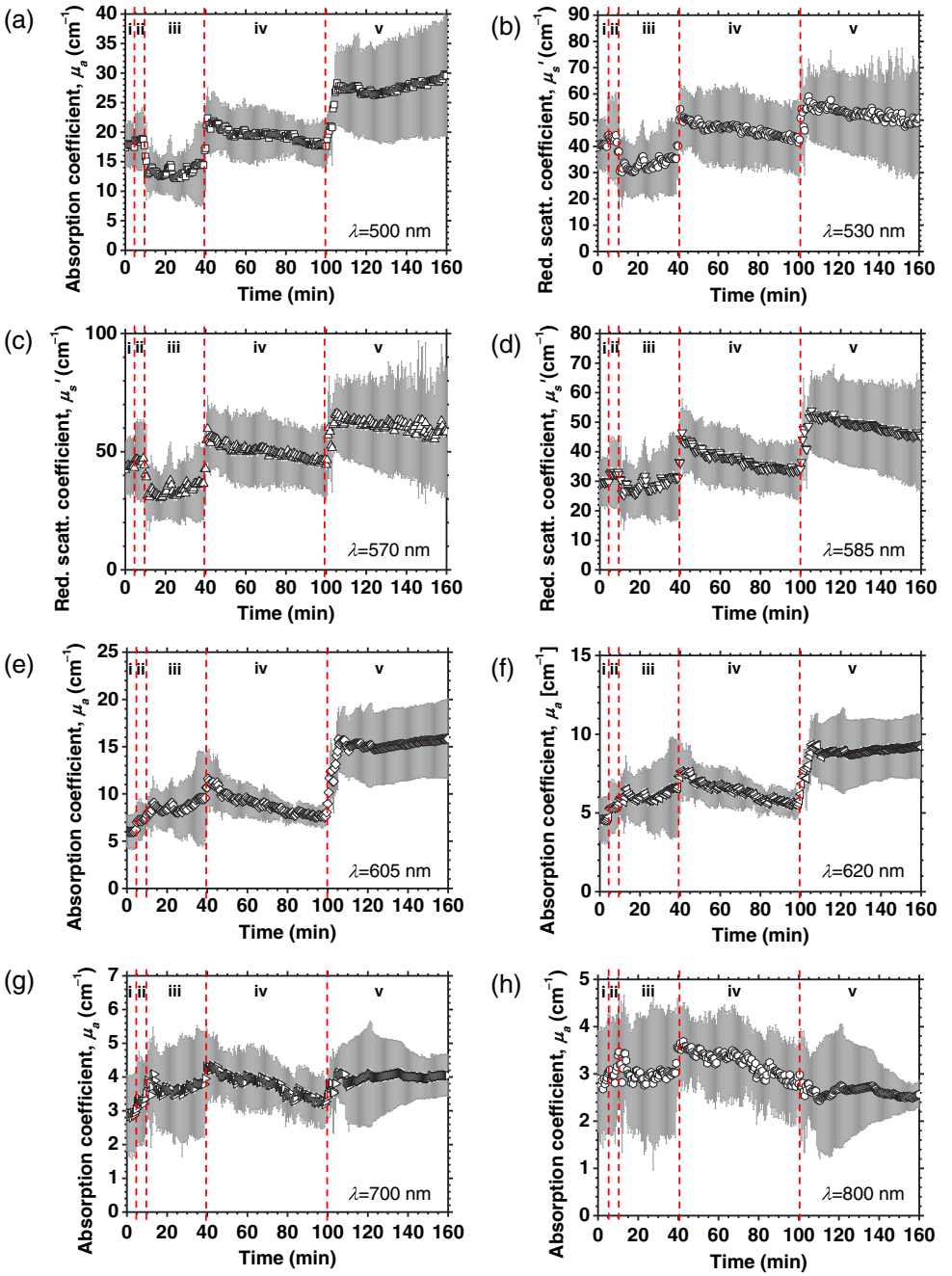

Fig. 7 Time courses of the absorption coefficient μ_a averaged over six samples during ischemia–reperfusion experiments at (a) 500 nm, (b) 530 nm, (c) 570 nm, (d) 584 nm, (e) 605 nm, (f) 620 nm, (g) 700 nm, and (h) 800 nm. The error bars represent the standard deviation over six samples ($n = 6$). In each figure, i, ii, iii, iv, and v indicate O_2-breathing, air-breathing, ischemia under air-breathing, reperfusion under air-breathing, and N_2-breathing, respectively.

Table 1 Absorption coefficient μ_a of *in vivo* rat liver tissue at specific wavelengths averaged over the period of oxygen breathing, air breathing, ischemia, reperfusion, and nitrogen breathing. Values are presented as mean ± standard deviation (SD) for each period. An unpaired *t*-test revealed the significant differences between air breathing and the other conditions.

$\mu_a(\lambda)$ (cm^{-1})	O_2 breathing	Air breathing	Ischemia	Reperfusion	N_2 breathing
500 nm	17.77 ± 0.20*	18.48 ± 0.32	13.48 ± 0.95*	19.51 ± 1.03*	27.08 ± 2.04*
530 nm	30.89 ± 0.48	31.41 ± 0.99	19.81 ± 1.71*	33.15 ± 1.98*	47.85 ± 4.17*
570 nm	34.31 ± 0.61	35.07 ± 1.07	21.55 ± 2.20*	37.85 ± 2.63*	59.18 ± 5.75*
584 nm	20.40 ± 0.26*	21.93 ± 0.49	16.47 ± 1.67*	25.21 ± 2.47*	44.32 ± 4.42*
605 nm	6.03 ± 0.08*	7.23 ± 0.13	8.66 ± 0.56*	8.88 ± 1.05*	14.99 ± 1.09*
620 nm	4.60 ± 0.07*	5.40 ± 0.10	6.14 ± 0.31*	6.36 ± 0.60*	8.86 ± 0.48*
700 nm	2.90 ± 0.07*	3.31 ± 0.09	3.70 ± 0.16*	3.77 ± 0.31*	3.98 ± 0.11*
800 nm	2.82 ± 0.08*	3.00 ± 0.10	3.02 ± 0.17	3.24 ± 0.24*	2.62 ± 0.09*

Note: *$P < 0.05$

than at the other wavelengths, which coincides with the absorption spectrum of hemoglobin.[39] The decrease in μ_a following the induction of ischemia and increase in μ_a after the restoration of blood circulation can be observed at 500, 530, 570, and 584 nm. These changes in μ_a are indicative of a decrease in total hemoglobin concentration because these wavelengths correspond to the isosbestic wavelengths of hemoglobin in the visible wavelength region. The occlusion of total blood inflow to the liver (except for the caudate lobe) resulted in a drop in μ_a from the baseline ($P < 0.05$) for 500, 530, 570, and 584 nm, and μ_a values were gradually recovered 60 min after the onset of reperfusion. *In vivo* liver tissues examined in the present study exhibited an absorption coefficient that was strongly related to the hemoglobin absorption spectra. The maximum baseline of μ_a was 36.02 ± 10.77 cm^{-1} at 570 nm and was 3.15 ± 1.10 cm^{-1} at 800 nm. We found a significant difference in μ_a between the normal and ischemic liver tissues ($P < 0.05$) for a wavelength range from 500 to 700 nm, between the normal and reperfused liver tissues ($P < 0.05$) for a wavelength range from 500 to 800 nm, and between the normal and anoxic liver tissues ($P < 0.05$) for a wavelength range from 500 to 800 nm, as shown in Table 1. In the NIR wavelength region, the changes in μ_a remain, but the μ_a value increases during the ischemic phase as compared to the baseline value. The decrease in μ_a during ischemia and gradual increase in μ_a following reperfusion in the visible wavelength region indicate that μ_a at the isosbestic wavelengths can be used as a parameter to evaluate the change in total hemoglobin concentration under the hepatic ischemia–reperfusion injury. The period between the onset of nitrogen breathing and respiratory arrest averaged over all six samples was 87 ± 77 s.

Figure 8 shows the time courses of μ_s' averaged over the six samples at specific wavelengths during the period of preischemia (oxygen breathing and air breathing), ischemia, reperfusion, and nitrogen breathing. The error bars in Fig. 8 represent the standard deviation over the six samples. The average values of μ_s' over the six samples at each wavelength are averaged over each period and are summarized in Table 2. Time courses of μ_s' are well correlated with those of μ_a in the wavelength range from 500 to 584 nm, which is probably due to scattering by red blood cells. The average values of μ_s' at 700 and 800 nm over the ischemia period were significantly ($P < 0.05$) higher than that over the air breathing period. On the other hand, the average values of μ_s' at 500, 530, 570, and 585 nm over the ischemia period decreased significantly ($P < 0.05$) as compared to the average values of μ_s' over the air breathing period, although the maximum value was recorded after the onset of nitrogen breathing.

Figure 9 shows the time courses of StO_2 averaged over six samples during the period of preischemia (oxygen breathing and air breathing), ischemia, reperfusion, and nitrogen breathing. The average values of StO_2 over each period are summarized in Table 3. A sharp decrease in StO_2 following induction of ischemia is clearly observed. Sixty minutes after the onset of reperfusion, the value of StO_2 recovered gradually but remained lower than the baseline StO_2. The StO_2 was 59.56 ± 1.58% during oxygen breathing, 45.14 ± 3.86% during normal air breathing before ischemia, 3.60 ± 3.53% after 30 min of ischemia, 33.35 ± 7.27% 60 min after reflow of blood to the liver, and 4.91 ± 3.40% 60 min after death. The downslope was linear over the entire 30-min period of ischemia. Hence, after 30 min of ischemia, the value of StO_2 decreased significantly from the baseline and increased gradually ($P < 0.05$) after 60 min of reperfusion compared to the ischemic value. Figure 10 shows the time courses of $\mu_a(605)/\mu_a(620)$ averaged over six samples during the period of preischemia (oxygen breathing and air breathing), ischemia, reperfusion, and nitrogen breathing. The average values of $\mu_a(605)/\mu_a(620)$ over each period are summarized in Table 4. The value of $\mu_a(605)/\mu_a(620)$ increased significantly after the onset of ischemia and reverted to the preischemic level after 30 min of reperfusion. The value of $\mu_a(605)/\mu_a(620)$ increased dramatically under hypoxia and reached the maximum level 10 min after the onset of nitrogen breathing.

5 Discussion

The experimental results revealed that μ_a decreased sharply after the onset of ischemia at the isosbestic wavelengths of hemoglobin in the visible wavelength region, which indicates the decrease in hemoglobin concentration in liver tissue due

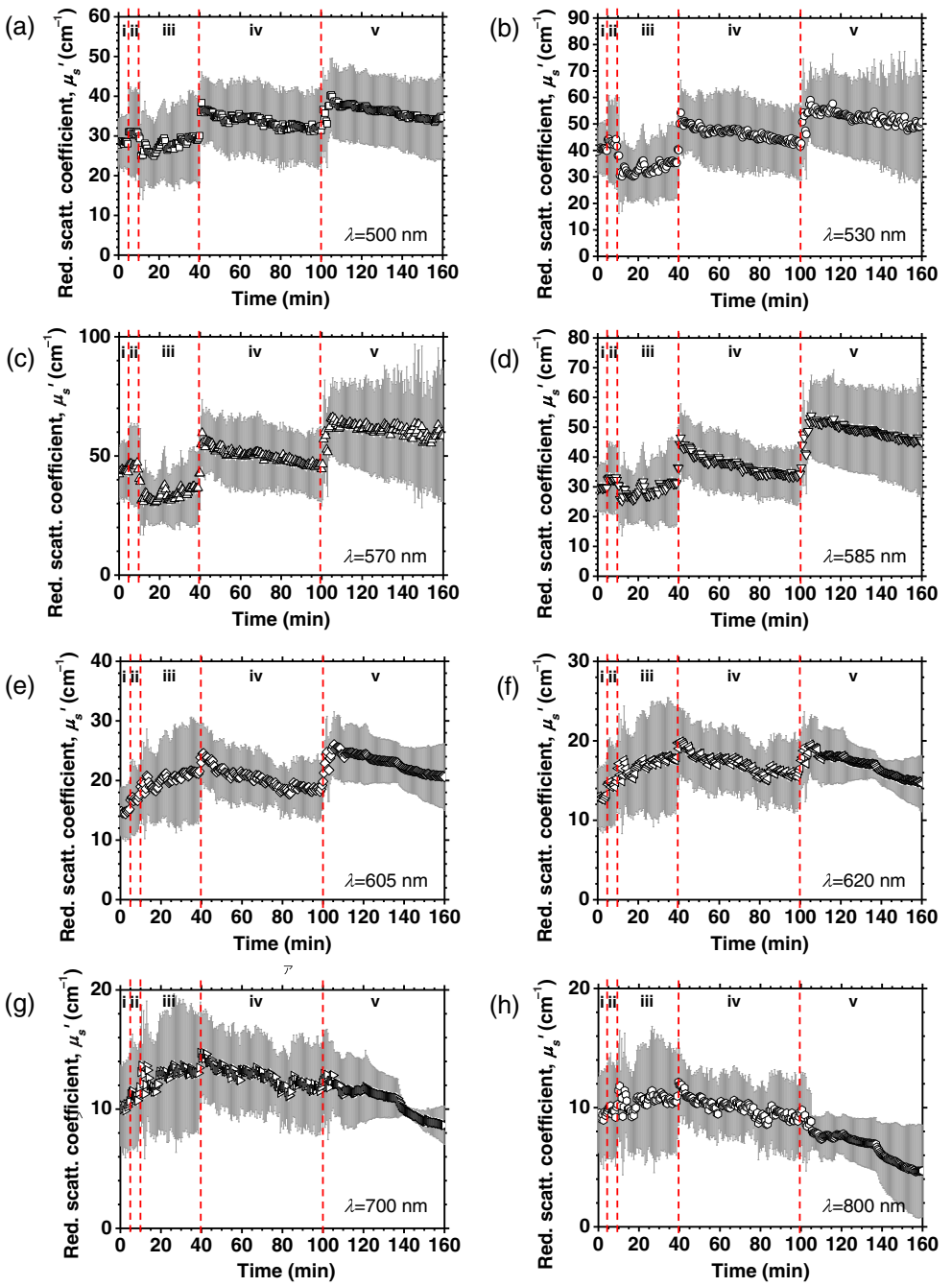

Fig. 8 Time courses of the absorption coefficient μ_s' averaged over six samples during ischemia–reperfusion experiments at (a) 500 nm, (b) 530 nm, (c) 570 nm, (d) 584 nm, (e) 605 nm, (f) 620 nm, (g) 700 nm, and (h) 800 nm. The error bars represent the standard deviation over six samples ($n = 6$). In each figure, i, ii, iii, iv, and v indicate O_2-breathing, air-breathing, ischemia under air-breathing, reperfusion under air-breathing, and N_2-breathing, respectively.

to the occlusion of the hepatic portal. The value of μ_a for *in vivo* liver tissue is primarily affected by the absorption properties of hemoglobin and CcO.[42] Since the hemoglobin absorbs light strongly in the wavelength range of 500 to 600 nm, the decrease in μ_a at 500, 530, 570, and 585 nm [Figs. 7(a)–7(d)] after the onset of ischemia is primarily reflected by the lower blood content of ischemic liver as compared to normal liver. The remarkable increase in μ_a at 500, 530, 570, and 585 nm is probably due to the increase in blood volume in the liver after death, which is consistent with the observations of increased liver weight in postmortem animals without immediate bleeding.[43–45] The change in StO_2 during ischemia and reperfusion was also reasonable, as shown in Fig. 9. The value of StO_2 decreased rapidly to $1.83 \pm 1.39\%$ after the onset of ischemia, whereas in the case of reperfusion, the value of StO_2 recovered up to $46.24 \pm 12.29\%$, which is as high as that before ischemia ($46.05 \pm 11.72\%$) under the normal condition with air breathing. The results showed that the current DRS system could effectively monitor the decrease in StO_2 resulting from the occlusion of blood inflow to the liver, which reflects the

Table 2 Absorption coefficient μ_s' of *in vivo* rat liver tissue at specific wavelengths averaged over the period of oxygen breathing, air breathing, ischemia, reperfusion, and nitrogen breathing. Values are presented as mean ± SD for each period. An unpaired *t*-test revealed the significant differences between air breathing and the other conditions.

$\mu_s'(\lambda)$ (cm^{-1})	O_2 breathing	Air breathing	Ischemia	Reperfusion	N_2 breathing
500 nm	28.32 ± 0.31*	30.76 ± 0.31	27.87 ± 1.60*	33.68 ± 1.53*	38.27 ± 1.63*
530 nm	40.53 ± 0.41*	43.13 ± 0.90	33.46 ± 2.21*	46.42 ± 2.33*	52.21 ± 2.67*
570 nm	43.64 ± 0.55*	46.13 ± 0.81	34.14 ± 2.61*	50.07 ± 2.94*	60.72 ± 3.26*
584 nm	29.64 ± 0.28*	32.62 ± 0.36	28.89 ± 2.13*	37.30 ± 3.07*	48.44 ± 3.00*
605 nm	14.75 ± 0.22*	16.96 ± 0.35	20.30 ± 1.12*	20.23 ± 1.65*	22.93 ± 1.53*
620 nm	12.90 ± 0.23*	14.60 ± 0.35	17.06 ± 0.90*	17.07 ± 1.16*	16.90 ± 1.34*
700 nm	10.25 ± 0.23*	11.23 ± 0.33	12.92 ± 0.65*	12.75 ± 0.81*	10.73 ± 1.22
800 nm	9.38 ± 0.25*	9.83 ± 0.33	10.60 ± 0.58*	9.98 ± 0.72	6.77 ± 1.29*

Note: *$P < 0.05$.

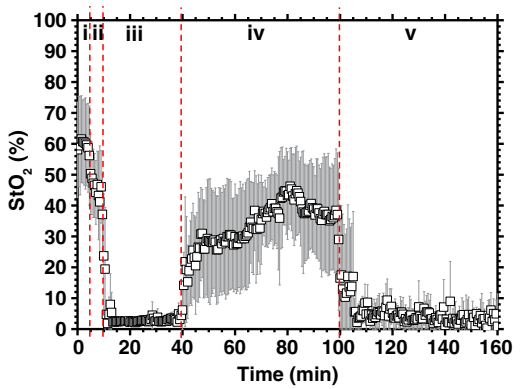

Fig. 9 Time course of the tissue oxygen saturation StO_2 averaged over six samples during ischemia–reperfusion experiments. The error bars represent the standard deviation over six samples ($n = 6$). In each figure, i, ii, iii, iv, and v represent O_2-breathing, air-breathing, ischemia under air-breathing, reperfusion under air-breathing, and N_2-breathing, respectively.

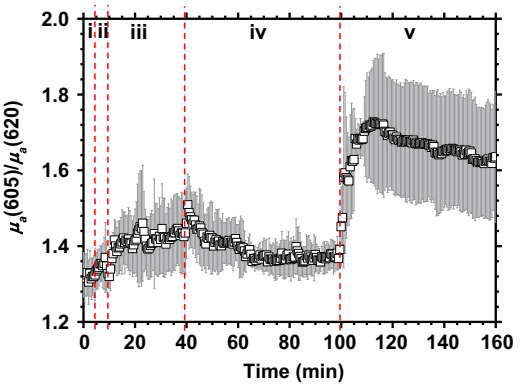

Fig. 10 Time course of the ratio of $\mu_a(605)$ and $\mu_a(620)$, averaged over six samples during ischemia–reperfusion experiments. The error bars represent the standard deviation over six samples ($n = 6$). In each figure, i, ii, iii, iv, and v represent O_2-breathing, air-breathing, ischemia under air-breathing, reperfusion under air-breathing, and N_2-breathing, respectively.

dysfunction of microcirculation in the liver induced by ischemia.[46] Hepatic ischemia–reperfusion injury reduces total hepatic blood flow and causes severe microcirculatory dysfunction, which results in venous stagnation, adversely affecting hepatic tissue oxygenation.[47] The decrease in HbO immediately after occlusion of the hepatic portal vein resulted in a decrease in the StO_2 level. At the end of the reperfusion period, HbO levels recovered, which helps to increase StO_2 following reperfusion.[47] We also observed significant increases in $\mu_a(605)/\mu_a(620)$ during ischemia and after the onset of nitrogen breathing (Fig. 10), representing a reduction in heme *aa*3, which is a sign of mitochondrial energy failure. This is supported by the change in absorption spectrum of *in vitro* blood-free liver induced by the application of $Na_2S_2O_4$, as shown in Fig. 4. On the other hand, it has been reported that noninvasive optical evaluation of CcO redox state *in vivo* can suffer from optical cross talk from hemoglobin absorption signals.[48,49] Hence, the measurements of heme aa_3 in CcO based on the value of

Table 3 Tissue oxygen saturation StO_2 of *in vivo* rat liver tissue at specific wavelengths averaged over the period of oxygen breathing, air breathing, ischemia, reperfusion, and nitrogen breathing. Values are presented as mean ± SD for each period. An unpaired *t*-test revealed the significant differences between air breathing and the other conditions.

	O_2 breathing	Air breathing	Ischemia	Reperfusion	N_2 breathing
StO_2 (%)	59.56 ± 1.58*	45.14 ± 3.86	3.60 ± 3.53*	33.35 ± 7.27*	4.91 ± 3.40*

Note: *$P < 0.05$.

Table 4 Ratio $\mu_a(605)/\mu_a(620)$ of *in vivo* rat liver tissue at specific wavelengths averaged over the period of oxygen breathing, air breathing, ischemia, reperfusion, and nitrogen breathing. Values are presented as mean ± SD for each period. An unpaired *t*-test revealed the significant differences between air breathing and the other conditions.

	O_2 breathing	Air breathing	Ischemia	Reperfusion	N_2 breathing
$\mu_a(605)/\mu_a(620)$	1.32 ± 0.01*	1.35 ± 0.01	1.42 ± 0.02*	1.39 ± 0.03*	1.66 ± 0.04*

Note: *$P < 0.05$.

$\mu_a(605)/\mu_a(620)$ could be varied with the changes in the concentrations of oxygenated and deoxygenated hemoglobin. However, the possibility of relative measurements of the redox state of heme aa_3 in CcO of *in vivo* rat liver could still prove valuable. Studies on the multiple regression analysis for the estimated $\mu_a(\lambda)$ with the extinction coefficient spectra of oxygenated hemoglobin, deoxygenated hemoglobin, oxidized heme aa_3, and reduced heme aa_3 would strengthen the method in the future. We will investigate the multiple regression analysis for $\mu_a(\lambda)$ involving those four chromophores further in future work.

It has been reported that ischemia–reperfusion may cause postischemic microvascular reperfusion failure,[50] which is characterized by a reduction in sinusoidal red blood cell velocity,[51] ultimately affecting μ_a and μ_s'. The value of μ_s' for *in vivo* liver tissue is affected by light scattering by cellular structures in tissues and red blood cells in microcirculation. The changes in light scattering at 500, 530, 570, and 584 nm [Figs. 8(a)–8(d)] reflect that scattering is strongly affected by red blood cells and is well synchronized with the absorption changes of corresponding wavelengths [Figs. 7(a)–7(d)]. By contrast, the light scattering in the NIR wavelength region [Figs. 8(g) and 8(h)] is primarily affected by changes in tissue morphology. The changes in μ_s' in the NIR region during the experiments were quite different from those at the isosbestic wavelengths of hemoglobin in the visible wavelength region. The spectrum of the reduced scattering coefficient $\mu_s'(\lambda)$ of biological tissues can be treated as a combination of $\mu_s'(\lambda)$ for cellular and subcellular structures of different sizes.[52] Generally, the sizes of the cellular and subcellular structures in biological tissues are distributed as follows: membranes, <0.01 μm;[53] ribosomes, <0.01 μm;[54] vesicles, 0.1 to 0.5 μm;[53] lysosomes, 0.1 to 0.5 μm;[55] mitochondria, 1 to 2 μm;[52] nuclei, 5 to 10 μm;[52] and cells, 5 to 75 μm.[52] Figure 11 shows the spectra of the reduced scattering coefficient $\mu_s'(\lambda)$ calculated by the Mie theory for spheres of various sizes. In the Mie-theory based calculation, the refractive indices of a sphere and the surrounding medium were set to be 1.46 and 1.35, respectively, at a volume concentration of 2%. The slope of $\mu_s'(\lambda)$ decreases as the diameter of the sphere d increases. The entire spectrum of $\mu_s'(\lambda)$ increases as the diameter of the sphere d increases in the range of $d = 0.01$ to 0.2 μm, but decreases as the diameter of the sphere d increases in the range of $d = 0.6$ to 10.0 μm.

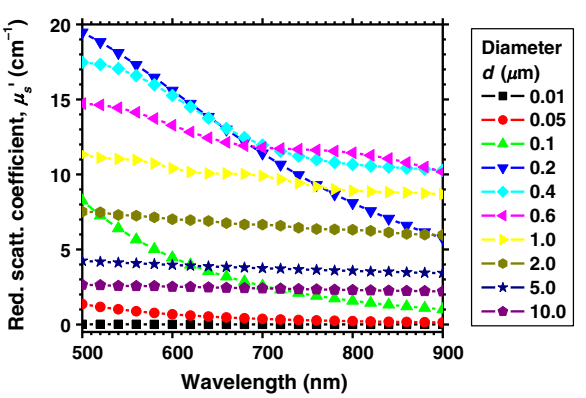

Fig. 11 Reduced scattering coefficient $\mu_s'(\lambda)$ calculated by the Mie theory for spheres of various sizes.

Anoxia has been reported to induce postmortem hepatocyte vacuolation and liver weight increase.[43,44] Pronounced hepatocyte vacuolation can occur as soon as 30 s after the suspension of organ perfusion *in vitro* or up to 3 to 4 min after death under an anoxic condition.[43,44] The hepatocyte vacuoles are single or multiple and round or oval, and are often well demarcated, with variable displacement of hepatocyte nuclei. Some vacuoles are clear, but most have pale or eosinophilic contents with a homogeneous, granular, and/or fibrillary appearance. A mixed clear/eosinophilic stained appearance has been frequently observed within a single vacuole or vacuoles in the same hepatocyte. Intracytoplasmic vacuoles increased in size and number, and hepatocyte vacuolation and sinusoidal congestion extended from more centrilobular to periportal regions as the postmortem interval increased.[45] Several studies demonstrated that hepatocyte vacuoles for rats were 2 to 15 μm in diameter within 15 min after death[43,44] or up to 25 μm in diameter 25 min after death.[45] As shown in Fig. 11, the volume increase in structures larger than 0.6 μm contributes to the decrease in μ_s' in the NIR wavelength region. Therefore, the decrease in $\mu_s'(\lambda)$ in the NIR wavelength region after the onset of nitrogen breathing or pulmonary arrest obtained by the proposed method indicates hepatocyte vacuolation. This implies that the irreversible morphological changes due to the loss of hepatic viability can be evaluated using the reduced scattering coefficients estimated by the current DRS system. The causes of the temporary increase of μ_s' in the NIR region during ischemia remain unclear. One possible explanation for such a reversible scattering change is the volume changes in structures smaller than 0.2 μm (membranes, ribosomes, small vesicles, and mitochondrial matrix granules), as shown in Fig. 11. The severity of hepatocyte damage has been reported to depend on the length of warm ischemia.[56,57] Short periods of ischemia result in reversible cell injury, in which liver oxygen consumption reverts to normal levels when oxygen is resupplied during reperfusion. Reperfusion after more prolonged periods of ischemia (2 to 3 h) results in irreversible cell damage. The time limit for hepatocytes survival was estimated to be 1.5 h of warm ischemia.[56,57] It has also been reported that as an ischemia–reperfusion injury, necrosis and apoptosis occur 3 to 6 h after ischemia–reperfusion.[58] The scattering changes in the NIR wavelength region during reperfusion for at least 6 h after more prolonged periods of ischemia should be investigated in the future. Liver transplantation would be one useful clinical application of this technology because

an adequate blood supply and tissue oxygenation of the graft is essential to its initial function.[59,60] The results for $\mu_a(\lambda)$, $\mu_s'(\lambda)$, StO_2, and $\mu_a(605)/\mu_a(620)$ indicate that the method applied in the present study is reliable and has potential application in the intraoperative assessment of graft tissue viability.

6 Conclusions

We investigated a method for evaluating the reduced scattering coefficient, the absorption coefficient, the tissue oxygen saturation, and the reduction of heme *aa*3 of *in vivo* liver tissue using a single-reflectance fiber probe with two source-collector geometries. The time courses of μ_a at 500, 530, 570, and 584 nm indicated the hemodynamic change in the liver tissue as well as StO_2. A significant increase in $\mu_a(605)/\mu_a(620)$ during ischemia and after euthanasia induced by nitrogen breathing was observed, indicating a reduction in heme *aa*3, which is a sign of mitochondrial energy failure. The time courses of μ_s' at 500, 530, 570, and 584 nm were well correlated with those of μ_a, which also reflects the scattering by red blood cells. On the other hand, at 700 and 800 nm, a temporary increase in μ_s' and an irreversible decrease in μ_s' were observed during ischemia–reperfusion and after euthanasia induced by nitrogen breathing, respectively. The change in μ_s' in the NIR wavelength region during ischemia is indicative of the morphological changes in the cellular and subcellular structures induced by ischemia, whereas that after euthanasia implies hepatocyte vacuolation. The results of the present study indicate the potential application of the current DRS system in evaluating the pathophysiological conditions of *in vivo* liver tissue. The advantages of the proposed method are its simplicity and portability, because the only devices required are a white light source, fiber optics, and two spectrometers. Since the proposed method can be used to simultaneously evaluate changes in hemodynamics, mitochondrial energy level, and tissue morphology, this method will be useful for studying tissue viability of *in vivo* liver tissue. We intend to further extend the proposed method in order to investigate pathophysiological conditions of liver tissue, such as those resulting from liver transplantation.

References

1. J. W. Kupiec-Weglinski and R.W. Busuttil, "Ischemia and reperfusion injury in liver transplantation," *Transplant. Proc.* **37**(4), 1653–1656 (2005).
2. J. H. Pringle, "Notes on the arrest of hepatic hemorrhage due to trauma," *Ann. Surg.* **48**(4), 541–549 (1908).
3. M. Kretzschmar, A. Krüger, and W. Schirrmeister, "Hepatic ischemia–reperfusion syndrome after partial liver resection (LR): hepatic venous oxygen saturation, enzyme pattern, reduced and oxidized glutathione, procalcitonin and interleukin-6," *Exp. Toxicol. Pathol.* **54**(5–6), 423–431 (2003).
4. S. H. Tseng et al., "Noninvasive evaluation of collagen and hemoglobin contents and scattering property of in vivo keloid scars and normal skin using diffuse reflectance spectroscopy: pilot study," *J. Biomed. Opt.* **17**(7) 077005 (2012).
5. D. Fabila et al., "In vivo assessment of liver fibrosis using diffuse reflectance and fluorescence spectroscopy: a proof of concept," *Photodiagn. Photodyn. Ther.* **9**(4), 376–382 (2012).
6. T. Kitai et al., "Intraoperative measurement of the graft oxygenation state in living related liver transplantation by near infrared spectroscopy," *Transplant. Int.* **8**(2), 111–118 (1995).
7. T. Kitai et al., "Quantitative detection of hemoglobin saturation in the liver with near-infrared spectroscopy," *Hepatology* **18**(4), 926–936 (1993).
8. L.-H. Wang, S. L. Jacques, and L.-Q. Zheng, "MCML-Monte Carlo modeling of photon transport in multi-layered tissues," *Comput. Methods Programs Biomed.* **47**(2), 131–146 (1995).
9. A. E. EI-Desoky et al., "Assessment of hepatic ischaemia–reperfusion injury by measuring intracellular tissue oxygenation using near infrared spectroscopy," *Liver* **21**(1), 37–44 (2001).
10. L. Sikurova, P. Balis, and M. Zvarik, "Penetration of laser light through red blood cell ghosts," *J. Photochem. Photobiol. B.* **103**(3), 230–233 (2011).
11. R. Nachabé et al., "Estimation of lipid and water concentrations in scattering media with diffuse optical spectroscopy from 900 to 1,600 nm," *J. Biomed. Opt.* **15**(3), 037015 (2010).
12. D. J. Evers et al., "Optical sensing for tumor detection in the liver," *Eur. J. Surg. Oncol.* **39**(1), 68–75 (2013).
13. Y. Fawzy et al., "In vivo assessment and evaluation of lung tissue morphologic and physiological changes from noncontact endoscopic reflectance spectroscopy for improving lung cancer detection," *J. Biomed. Opt.* **11**(4), 044003 (2006).
14. M. S. Patterson, B. Chance, and B. C. Wilson, "Time resolved reflectance and transmittance for the noninvasive measurement of tissue optical properties," *Appl. Opt.* **28**(12), 2331–2336 (1989).
15. J. B. Fishkin et al., "Frequency-domain photon migration measurements of normal and malignant tissue optical properties in a human subject," *Appl. Opt.* **36**(1), 10–20 (1997).
16. G. Yoon, D. N. Ghosh Roy, and R. C. Straight, "Coherent backscattering in biological media: measurement and estimation of optical properties," *Appl. Opt.* **32**(4) 580–585 (1993).
17. S. A. Prahl and I. A. Vitkin, "Determination of optical properties of turbid media using pulsed photothermal radiometry," *Phys. Med. Biol.* **37**(6) 1203–1217 (1992).
18. T. J. Farrell, M. S. Patterson, and B. Wilson, "A diffusion theory model of spatially resolved, steady-state diffuse reflectance for the noninvasive determination of tissue optical properties in vivo," *Med. Phys.* **19**(4), 879–888 (1992).
19. L. Wang and S. L. Jacques, "Use of a laser beam with an oblique angle on incidence to measure the reduced scattering coefficient of a turbid medium," *Appl. Opt.* **34**(13), 2362–2366 (1995).
20. A. Kienle et al., "Spatially resolved absolute diffuse reflectance measurements for noninvasive determination of the optical scattering and absorption coefficients of biological tissue," *Appl. Opt.* **35**(13), 2304–2314 (1996).
21. S.-P. Lin et al., "Measurement of tissue optical properties by the use of oblique-incidence optical fiber reflectometry," *Appl. Opt.* **36**(1), 136–143 (1997).
22. T. M. Bydlon et al., "Chromophore based analyses of steady-state diffuse reflectance spectroscopy: current status and perspectivesfor clinical adoption," *J. Biophotonics* **8**(1–2), 9–24 (2015).
23. S. Kennedy et al., "Optical breast cancer margin assessment: an observational study of the effects of tissue heterogeneity on optical contrast," *Breast Cancer Res.* **12**(6), R91 (2010).
24. M. D. Keller et al., "Autofluorescence and diffuse reflectance spectroscopy and spectral imaging for breast surgical margin analysis," *Lasers Surg. Med.* **42**(1), 15–23 (2010).
25. J. Brown et al., "Quantitative optical spectroscopy: a robust tool for direct measurement of breast cancer vascular oxygenation and total hemoglobin content in vivo," *Cancer Res.* **69**(7), 2919–2926 (2009).
26. P. R. Bargo et al., "In vivo determination of optical properties of normal and tumor tissue with white light reflectance and empirical light transport model during endoscopy," *J. Biomed. Opt.* **10**(3), 034018 (2005).
27. S. Kawauchi et al., "Simultaneous measurement of changes in light absorption due to the reduction of cytochrome c oxidase and light scattering in rat brains during loss of tissue viability," *Appl. Opt.* **47**(22), 4164–4176 (2008).
28. C. Hsu et al., "Liver tumor gross margin identification and ablation monitoring during liver radiofrequency treatment," *J. Vasc. Interv. Radiol.* **16**(11), 1473–1478 (2005).
29. S. Wong, P. Mangu, and M. Choti, "American Society of Clinical Oncology 2009 clinical evidence review on radiofrequency ablation of hepatic metastases from colorectal cancer," *J. Clin. Oncol.* **28**(3), 493–508 (2010).

30. T. M. Pawlik et al., "Effect of surgical margin status on survival and site of recurrence after hepatic resection for colorectal metastases," *Ann. Surg.* **241**(5), 715–722 (2005).
31. B. Nordlinger et al., "Perioperative chemotherapy with FOLFOX4 and surgery versus surgery alone for resectable liver metastases from colorectal cancer (EORTC Intergroup trial 40983): a randomised controlled trial," *Lancet* **371**(9617), 1007–1016 (2008).
32. A. Muratore et al., "Resection margin and recurrence-free survival after liver resection of colorectal metastases," *Ann. Surg. Oncol.* **17**(5), 1324–1329 (2010).
33. B. R. Karakas et al., "Investigating viability of intestine using spectroscopy: a pilot study," *J. Surg. Res.* **191**(1) 91–8 (2014).
34. B. Yu et al., "Diffuse reflectance spectroscopy with a self-calibrating fiber optic probe," *Opt. Lett.* **33**(16), 1783–1785 (2008).
35. J. Y. Lo et al., "A strategy for quantitative spectral imaging of tissue absorption and scattering using light emitting diodes and photodiodes," *Opt. Express* **17**(3), 1372–1384 (2009).
36. A. Kim et al., "A fiber optic reflectance probe with multiple source-collector separations to increase the dynamic range of derived tissue optical absorption and scattering coefficients," *Opt. Express* **18**(6), 5580–5594 (2010).
37. I. Nishidate et al., "In vivo estimation of light scattering and absorption properties of rat brain using a single-reflectance fiber probe during cortical spreading depression," *J. Biomed. Opt.* **20**(2), 027003 (2015).
38. H. J. van Staveren et al., "Light scattering in Intralipid-10% in the wavelength range of 400–1100 nm," *Appl. Opt.* **30**(31), 4507–4514 (1991).
39. S. A. Prahl, "Tabulated molar extinction coefficient for hemoglobin in water," http://omlc.ogi.edu/spectra/hemoglobin/summary.html (1999).
40. D. C. Wharton and A. Tzagoloff, "Studies on the electron transfer system. LVII. The near infrared absorption band of cytochrome oxidase," *J. Biol. Chem.* **239**(6), 2036–2041 (1964).
41. J. H. Dong et al., "Tolerance limit of rats to normothermic hepatic inflow occlusion under portal blood bypass," *Hepatobiliary Pancreat. Dis. Int.* **1**(1), 57–62 (2002).
42. T. Kitai et al., "Application of near-infrared time-resolved spectroscopy to rat liver—a preliminary report for surgical application," *Phys. Med. Biol.* **44**(8), 2049–2061 (1999).
43. B. I. Sykes, E. Penny, and F. H. Purchase, "Hepatocyte vacuolation and increased liver weight occurring in anoxic rat," *Toxicol. Appl. Pharmacol.* **36**, 31–39 (1976).
44. O. A. Trowell, "The experimental production of watery vacuolation of the liver," *J. Physiol.* **105**, 268–297 (1946).
45. X. Li et al., "Morphogenesis of postmortem hepatocyte vacuolation and liver weight increases in Sprague-Dawley rats," *Toxicol. Pathol.* **31**, 682–688 (2003).
46. C. H. Li et al., "The monitoring of microvascular liver blood flow changes during ischemia and reperfusion using laser speckle contrast imaging," *Microvasc. Res.* **94**, 28–35 (2014).
47. C. K. Sun et al., "Effect of ischemia–reperfusion injury on the microcirculation of the steatotic liver of the Zucker rat," *Transplantation* **72**(10), 1625–1631 (2001).
48. C. E. Cooper and R. Springett, "Measurement of cytochrome oxidase and mitochondrial energetics by near-infrared spectroscopy," *Philos. Trans. R. Soc.* **B352**(1354), 669–676 (1997).
49. C. E. Cooper et al., "Measurement of cytochrome oxidase redox state by near infrared spectroscopy," *Adv. Exp. Med. Biol.* **413**, 63–73 (1997).
50. T. Kondo et al., "Impact of ischemia–reperfusion injury on dimensional changes of hepatic microvessels," *Res. Exp. Med.* **198**(2), 63–72 (1998).
51. B. Vollmar et al., "Role of microcirculatory derangements in manifestation of portal triad cross-clamping-induced hepatic reperfusion injury," *J. Surg. Res.* **60**(1), 49–54 (1996).
52. V. Tuchin, *Tissue Optics: Light Scattering Methods and Instruments for Medical Diagnosis*, 2nd ed., SPIE Press, Bellingham, Washington (2007).
53. S. L. Jacques and S. A. Prahl, "Some biological scatteres," 1998, http://omlc.org/classroom/ece532/class3/scatterers.html (13 August 2014).
54. H. Fang et al., "Noninvasive sizing of subcellular organelles with light scattering spectroscopy," *IEEE J. Sel. Top. Quantum Electron.* **9**(2), 267–276 (2003).
55. J. R. Mourant et al., "Mechanisms of light scattering from biological cells relevant to noninvasive optical-diagnostics," *Appl. Opt.* **37**(16), 3586–3593 (1998).
56. C. Peralta, M. B. Jiménez-Castro, and J. Gracia-Sancho, "Hepatic ischemia and reperfusion injury: effects on the liver sinusoidal milieu," *J. Hepatol.* **59**(5), 1094–106 (2013).
57. B. González-Flecha, J. C. Cutrin, and A. Boveris, "Time course and mechanism of oxidative stress and tissue damage in rat liver subjected to in vivo ischemia–reperfusion," *J. Clin. Invest.* **91**(2), 456–464 (1993).
58. S. Suzuki, L. H. Toledo-Pereyra, and F. J. Rodriguez, "Role of neutrophils during the first 24 hours after liver ischemia and reperfusion injury," *Transplant. Proc.* **26**(6), 3695–3700 (1994).
59. R. M. Goldstein et al., "Problematic vascular reconstruction in liver transplantation. Part I. Arterial," *Surgery* **107**(5) 540–543 (1990).
60. D. M. Payen et al., "Portal and hepatic arterial blood flow measurement of human transplanted livers by implanted Doppler probes: interest for early complications and nutrition," *Surgery* **107**(4), 540–543 (1990).

Biographies for the authors are not available.